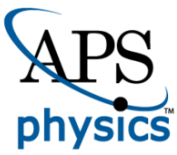

Impact of a resonance on thermal targets for invisible dark photon searches

Jonathan L. Feng and Jordan Smolinsky

Phys. Rev. D **96**, 095022 — Published 20 November 2017

DOI: 10.1103/PhysRevD.96.095022

Impact of Resonance on Thermal Targets for Invisible Dark Photon Searches

Jonathan L. Feng* and Jordan Smolinsky†
Department of Physics and Astronomy, University of California, Irvine, California 92697-4575 USA

Dark photons in the MeV to GeV mass range are important targets for experimental searches. We consider the case where dark photons A' decay invisibly to hidden dark matter X through $A' \to XX$. For generic masses, proposed accelerator searches are projected to probe the thermal target region of parameter space, where the X particles annihilate through $XX \to A' \to$ SM in the early universe and freeze out with the correct relic density. However, if $m_{A'} \approx 2m_X$, dark matter annihilation is resonantly enhanced, shifting the thermal target region to weaker couplings. For $\sim 10\%$ degeneracies, we find that the annihilation cross section is generically enhanced by four (two) orders of magnitude for scalar (pseudo-Dirac) dark matter. For such moderate degeneracies, the thermal target region drops to weak couplings beyond the reach of all proposed accelerator experiments in the scalar case and becomes extremely challenging in the pseudo-Dirac case. Proposed direct detection experiments can probe moderate degeneracies in the scalar case. For greater degeneracies, the effect of the resonance can be even more significant, and both scalar and pseudo-Dirac cases are beyond the reach of all proposed accelerator and direct detection experiments. For scalar dark matter, we find an absolute minimum that sets the ultimate experimental sensitivity required to probe the entire thermal target parameter space, but for pseudo-Dirac fermions, we find no such thermal target floor.

I. INTRODUCTION

The universe appears to be filled with dark matter with a relic density of $\Omega_X h^2 = 0.1199 \pm 0.0022$, where Ω_X is the energy density of dark matter in units of the critical density, and $h \simeq 0.67$ is the reduced Hubble parameter [1]. Because the relic density is an important quantity and so precisely known, or perhaps because so little else is known about dark matter, scenarios in which dark matter is produced through a simple mechanism that gives the correct Ω_X attract special attention. In particular, dark matter that begins in thermal equilibrium with the standard model and then freezes out with the correct thermal relic density is often considered especially well motivated. Examples include weakly-interacting massive particles (WIMPs), weak-scale particles with weak interactions, and WIMPless dark matter [2], hidden sector particles that are lighter and more weakly-coupled than WIMPs (or heavier and more strongly-coupled than WIMPs), but nevertheless also have the correct thermal relic abundance. For both WIMP and WIMPless dark matter, the region of parameter space that yields the correct thermal relic density, often known as the "thermal target," provides a useful goal for current and proposed experimental searches.

* jlf@uci.edu
† jsmolins@uci.edu

Dark photon models [3–6] are a simple and elegant realization of the WIMPless possibility. Dark photons A' are light gauge bosons that have coupling g_X to dark matter X in the hidden sector and couplings κq_f to standard model particles f, where κ is the kinetic mixing parameter, and q_f is the electric charge of f. The dark matter's relic density is determined by the annihilation process $XX \to A' \to \text{SM}$, and for particular choices of m_X, $m_{A'}$, g_X, and κ, this annihilation process yields the correct thermal relic density.

Typically, one considers $g_X \sim 1$ and $\kappa \ll 1$, where κ is assumed to be suppressed, because it is generated at loop level. The dark photon scenario then splits into two cases. If $m_{A'} < 2m_X$, dark photons always decay to the visible (standard model) sector. In this case, dark photons are produced at accelerators through their interactions with standard model particles and decay back to standard model particles. They mediate a new force, a revolutionary discovery in and of itself, but their implications for dark matter are not directly probed by accelerator experiments.

If $m_{A'} > 2m_X$, however, dark photons produced at accelerators typically decay invisibly to the hidden sector through $A' \to XX$. In this case, experiments that produce dark photons also produce dark matter, and the signature is missing mass, energy, or momentum. Of course, there is a long road ahead to identify the missing particle with the dark matter that permeates the universe, but at least in this case, the underlying process involves a dark matter candidate. The number and variety of experiments that are potentially sensitive to invisibly-decaying dark photons is staggering. They include BaBar [7, 8], CRESST II [9], E137 [10, 11], LSND [11–14], and NA64 [15], which currently bound various regions of parameter space, and BDX [11, 16, 17], Belle II [18], COHERENT [19, 20], DarkLight [21], LDMX [22], MiniBoone [11, 13, 14, 23], MMAPS [24], NA64 [25], PADME [26, 27], SHiP [28, 29], SBNe/SBNπ [30, 31], and VEPP-3 [32], which will probe this scenario in the future. The promise of discovering a portal to the dark sector in these experiments is significant, especially in the case of LDMX, which has been projected to probe all of the thermal target region for MeV $< m_X \lesssim$ GeV, $m_{A'} \gtrsim 3m_X$, and $g_X \sim 1$ [33]. In addition, a large number of direct detection experiments, which we discuss below, although not creating real dark photons, also probe these scenarios through $X\,\text{SM} \to X\,\text{SM}$ mediated by a t-channel A', where the $A'XX$ interaction is the same one that mediates the dark photon's invisible decays.

The invisible decay case with $m_{A'} > 2m_X$ is, however, also the "half" of parameter space in which dark matter annihilation may be resonantly enhanced. This has been noted previously, for example, in Ref. [33] (see, in particular, the supplementary material), but the impact of the A' resonance has not been investigated in detail. For degeneracies $0 < m_{A'} - 2m_X \lesssim T_f$, where T_f is the temperature at freezeout, the kinetic energy of dark matter particles can put the annihilation process $XX \to A' \to \text{SM}$ on resonance. As we will see, for $\sim 10\%$ degeneracies between $m_{A'}$ and $2m_X$, this resonance may have an extraordinary effect. For example, for scalar dark matter, the resonance generically raises the thermally-averaged annihilation cross section by four orders of magnitude. To compensate this kinematic enhancement, the thermal relic density may be corrected by lowering κ^2 by four orders of magnitude, but the resulting thermal target region of parameter space is then beyond the reach of any proposed accelerator experiment. Greater degeneracies move the thermal target to even weaker couplings.

In the following sections, we consider dark photon models with both scalar and pseudo-Dirac dark matter, estimate the effect of the resonance analytically, and present numerical results for the impact of the resonance on the thermal target region for a wide range of mass degeneracies.

II. DARK PHOTON MODEL

The dark photon model we consider is standard, but we present it here to establish notation and conventions. The hidden sector has a broken U(1) symmetry, and its massive gauge boson kinetically mixes with the standard model photon. In the mass basis, the resulting Lagrangian is

$$\mathcal{L} = -\frac{1}{4}F_{\mu\nu}F^{\mu\nu} - \frac{1}{4}F'_{\mu\nu}F'^{\mu\nu} + \frac{1}{2}m_{A'}^2 A'^2 + \sum_f \bar{f}(i\,\partial\!\!\!/ - eq_f A\!\!\!/ - \kappa eq_f A\!\!\!/' - m_f)f \ , \tag{1}$$

where $F_{\mu\nu}$ and $F'_{\mu\nu}$ are the field strengths of the photon A and dark photon A', respectively, $m_{A'}$ is the dark photon's mass, κ is the kinetic mixing parameter (we reserve ϵ for another quantity below), and f are standard model fermions with electric charges q_f and masses m_f.

The dark photon may decay to e^+e^- pairs throughout the parameter space we study. The decay width is

$$\Gamma_e \equiv \Gamma(A' \to e^+e^-) = \frac{\kappa^2 e^2 m_{A'}}{12\pi}\left[1 - \left(\frac{2m_e}{m_{A'}}\right)^2\right]^{1/2}\left[1 + \frac{2m_e^2}{m_{A'}^2}\right]. \tag{2}$$

For $m_{A'} > 2m_\mu$, decays to muons and a number of hadronic states are also possible. The full standard model decay

width is

$$\Gamma_{\rm SM} = \frac{\Gamma_e}{B_e(m_{A'})} \ , \tag{3}$$

where $B_e(m_{A'})$ is the branching fraction to e^+e^- pairs of a dark photon with mass $m_{A'}$, which may be extracted from measurements of $\sigma(e^+e^- \to e^+e^-)/\sigma^{\rm tot}_{e^+e^-}$ [34].

The hidden sector also contains the dark matter. We will consider both complex scalar [5] and pseudo-Dirac dark matter [11, 35, 36]. For the scalar case, the dark matter Lagrangian is

$$\mathcal{L}_\phi = \left|(\partial_\mu + i g_X A'_\mu)\phi\right|^2 - m_\phi^2 \left|\phi\right|^2 \ , \tag{4}$$

where ϕ is the scalar dark matter particle with mass m_ϕ, and $g_X = \sqrt{4\pi\alpha_X}$ is the hidden sector gauge coupling. In this case, the invisble (hidden sector) decay width is

$$\Gamma_\phi \equiv \Gamma(A' \to \phi\phi) = \frac{g_X^2 m_{A'}}{48\pi}\left[1 - \left(\frac{2m_\phi}{m_{A'}}\right)^2\right]^{3/2} \ . \tag{5}$$

For the pseudo-Dirac case, we consider a dark photon that couples to two hidden Weyl fermions that have a Dirac mass and small, identical Majorana masses. In the mass basis, the resulting dark matter Lagrangian is

$$\mathcal{L}_\chi = \sum_{i=1,2} \bar\chi_i (i\,\partial\!\!\!/ - m_i)\chi_i - (g_X \bar\chi_2 A\!\!\!/'\chi_1 + \text{h.c.}) \ , \tag{6}$$

where the two fermions χ_1 and χ_2 couple non-diagonally to the dark photon and have masses m_1 and m_2, respectively, with a small mass splitting $\Delta \equiv m_2 - m_1$. Below we will typically refer to χ_1 as the dark matter particle X with mass m_X and to χ_2 as the excited state with mass $m_X + \Delta$. In this pseudo-Dirac case, the invisible, hidden sector decay width is

$$\Gamma_\chi \equiv \Gamma(A' \to \chi_1\chi_2) = \frac{g_X^2 m_{A'}}{12\pi}\left[1 - \left(\frac{2m_X + \Delta}{m_{A'}}\right)^2\right]^{1/2}\left[1 + \frac{(2m_X+\Delta)^2}{2m_{A'}^2}\right]\left[1 - \frac{\Delta^2}{m_{A'}^2}\right]^{3/2} . \tag{7}$$

III. RELIC DENSITIES NEAR RESONANCE: ANALYTIC ESTIMATE

The formalism for treating dark matter annihilation near a resonance was developed long ago [37, 38]. In this section, we follow the method of Ref. [37] to derive a simple analytic estimate for the effect of a resonance on the thermal relic density for $\sim 10\%$ degeneracies. In Sec. IV, we will refine the standard treatment to improve its validity off resonance. We then use these results to derive more precise numerical results for cases with both more and less degeneracy, which we present in Sec. V.

The thermal relic abundance of a dark matter particle X is

$$\Omega_X h^2 = 8.77 \times 10^{-11}\ \text{GeV}^{-2}\left[\overline{g_{\rm eff}^{1/2}}\int_{x_f}^{x_0}\frac{\langle\sigma v\rangle}{x^2}dx\right]^{-1} \ , \tag{8}$$

where $\langle\sigma v\rangle$ is the thermally-averaged annihilation cross section, $x_0 = m_X/T_0 = 4.26 \times 10^{12}\ (m_X/\text{GeV})$, T_0 is the temperature now, and $x_f = m_X/T_f$, where T_f is the freezeout temperature. The freezeout temperature is found by solving the equation

$$\frac{63 \times 5^{1/2} x_f^{-1/2} e^{-x_f} g}{32\pi^3}\frac{g_{\rm eff}^{1/2}(x_f)}{h_{\rm eff}(x_f)} m_X m_{\rm Pl}\langle\sigma v\rangle = 1 \ . \tag{9}$$

In these equations, $g_{\rm eff}(x)$ and $h_{\rm eff}(x)$ are the effective numbers of degrees of freedom for energy and entropy density, respectively, $\overline{g_{\rm eff}^{1/2}}$ is the typical value of $g_{\rm eff}(x)$ between x_0 and x_f, and g is the number of X spin degrees of freedom.

To determine the thermal relic density, then, we must determine $\langle\sigma v\rangle$. In this section, we consider the simple case where the dark matter annihilates through the dark photon resonance $XX \to A' \to$ SM. For this case, it is convenient

to define

$$s_0 \equiv 4m_X^2 \tag{10}$$
$$\epsilon \equiv (s - s_0)/s_0 \tag{11}$$
$$\epsilon_R \equiv (m_{A'}^2 - s_0)/s_0 \tag{12}$$
$$\gamma_R \equiv m_{A'}\Gamma_{A'}/s_0 \ , \tag{13}$$

where ϵ, ϵ_R, and γ_R are dimensionless quantities that represent the kinetic energy of the collision, the kinetic energy required to be on resonance, and the width of the resonance, respectively. With a slight abuse of notation, in cases where it matters, for example, for the very small values of ϵ_R that we will consider below, these definitions should be considered to be in terms of physical quantities rather than Lagrangian parameters, so, for example, loop corrections have been included in the masses in Eqs. (10)–(13).

In general, $\langle\sigma v\rangle$ must be evaluated numerically, but the formalism simplifies greatly with three approximations. First, if the dark matter freezes out while non-relativistic, $x_f \equiv m_X/T_f \gg 1$, the thermally-averaged annihilation cross section is approximately [37]

$$\langle\sigma v\rangle_{\rm NR} = \frac{2x^{3/2}}{\pi^{1/2}}\int_0^\infty \sigma v_{\rm lab}\epsilon^{1/2}e^{-x\epsilon}d\epsilon \ , \tag{14}$$

where σ is the annihilation cross section, and

$$v_{\rm lab} = \frac{2\epsilon^{1/2}(1+\epsilon)^{1/2}}{1+2\epsilon} \tag{15}$$

is the relative velocity of the incoming particles in the rest frame of one of them. We have verified that $x_f \sim 15$ and the non-relativistic approximation is valid to $\sim 10\%$ throughout the regions of parameter space we consider.

Second, if we are sufficiently near the A' resonance, so $x_f\epsilon_R \lesssim 1$ or $m_{A'} - 2m_X \lesssim m_X/x_f$, we may take σ to have the Breit-Wigner form

$$\sigma_{\rm BW} = \frac{4\pi\omega}{p^2}B_iB_f\frac{m_{A'}^2\Gamma_{A'}^2}{(s-m_{A'}^2)^2+m_{A'}^2\Gamma_{A'}^2} = \frac{4\pi\omega}{m_X^2\epsilon}B_iB_f\frac{\gamma_R^2}{(\epsilon-\epsilon_R)^2+\gamma_R^2} \ , \tag{16}$$

where $\omega = (2S_{A'}+1)/(2S_X+1)^2$, $S_{A'}=1$ is the dark photon's spin, S_X is the dark matter's spin, and $B_i = B(A' \to XX)$ and $B_f = 1 - B_i = B(A' \to {\rm SM})$ are the branching fractions to the hidden and visible sectors, respectively.

Third, if the dark photon's couplings are sufficiently weak, so $\gamma_R \ll 1$ or $\Gamma_{A'} \ll m_{A'}$, we may use the narrow width approximation and the Breit-Wigner cross section becomes a delta function. In the numerical analysis described below in Sec. V, we have verified that, even for large $\alpha_X \sim 0.5$, the narrow width approximation gives thermally-averaged cross sections that are in agreement with the full result at the 10% level for $\epsilon_R \sim 0.1$, improving to 1% agreement for $\epsilon_R \lesssim 0.01$.

Given these three simplifications, the thermally-averaged annihilation cross section near a resonance at freezeout is [37]

$$\langle\sigma v\rangle_{\rm res} \approx \frac{16\pi^{3/2}\omega}{m_X^2}x_f^{3/2}\gamma_R B_iB_f\frac{(1+\epsilon_R)^{1/2}}{1+2\epsilon_R}e^{-x_f\epsilon_R} \tag{17}$$
$$\approx \frac{16\pi^{3/2}\omega}{m_X^2}x_f^{3/2}\frac{\Gamma_{A'}}{2m_X}B_iB_f e^{-x_f\epsilon_R} \ , \tag{18}$$

where in the last step we have used the fact that $x_f \sim 20$, and so the "near resonance" assumption implies $\epsilon_R \ll 1$. Since we are considering invisible decay scenarios, $B_i \approx 1$. We may also write $\Gamma_{A'}B_f = \Gamma_f \equiv N_f\kappa^2e^2m_X/12\pi$, where N_f is the effective number of kinematically accessible standard model decay channels. We then find that

$$\langle\sigma v\rangle_{\rm res} \approx \frac{2\pi^{1/2}\omega}{3m_X^2}x_f^{3/2}\kappa^2e^2N_fe^{-x_f\epsilon_R} \ . \tag{19}$$

In the absence of resonances, assuming $m_X \sim m_{A'}$, the typical value for the thermally-averaged annihilation cross section is

$$\langle\sigma v\rangle_{\text{non-res}} \sim \frac{\pi\kappa^2\alpha\alpha_X}{m_X^2}\frac{1}{x_f^L} = \frac{\kappa^2e^2g_X^2}{16\pi m_X^2}\frac{1}{x_f^L} \ , \tag{20}$$

where $L = 0$ (1) for s-wave (p-wave) annihilation. The nearby resonance therefore enhances the thermally-averaged annihilation cross section by a factor

$$\frac{\langle\sigma v\rangle_{\rm res}}{\langle\sigma v\rangle_{\rm non\text{-}res}} \sim \frac{32\pi^{3/2}\omega N_f}{3g_X^2} x_f^{3/2} x_f^L e^{-x_f\epsilon_R} \sim 5{,}000\ \frac{\omega N_f x_f^L e^{-x_f\epsilon_R}}{g_X^2}\ . \tag{21}$$

We see that a resonance may enhance the annihilation cross section (and suppress the thermal relic density) by four (two) orders of magnitude for the case of p-wave (s-wave) annihilators when $m_{A'}$ and $2m_X$ are degenerate to $\sim 10\%$.

This conclusion for the thermal relic density assumes $\Omega_X h^2 \sim \langle\sigma v\rangle^{-1}$, as typically follows from Eq. (8). This is valid for the $\sim 10\%$ degeneracies discussed here, but as we will see in Sec. V, for even greater degeneracies $\epsilon_R \ll 0.1$, there are additional effects that enhance the resonance effect further.

IV. RELIC DENSITIES NEAR RESONANCE: NUMERICAL ANALYSIS

In this section, we present our method for numerically evaluating the thermal relic density near resonance. Our numerical results assume dark matter is non-relativistic at freezeout, but unlike the analytic estimate of Sec. III, do not assume the resonance is nearby and do not assume the narrow-width approximation. In addition, we present results for both the scalar case and the pseudo-Dirac case. The method is a generalization of the treatment presented in Ref. [37].

The contribution of an s-channel resonance to the dark matter annihilation cross section can always be written in the form

$$\sigma v_{\rm lab} = F(\epsilon)\frac{m_{A'}\Gamma_{A'}}{(s-m_{A'}^2)^2 + m_{A'}^2\Gamma_{A'}^2}\ , \tag{22}$$

where $v_{\rm lab}$ is given in Eq. (15) and the dimensionless analytic function $F(\epsilon)$ encodes the cross section's dependence on the dimensionless kinetic energy $\epsilon \equiv (s-s_0)/s_0$, where $s_0 = 4m_X^2$ in the scalar case and $s_0 = (2m_X+\Delta)^2$ in the pseudo-Dirac case.

We can then exploit a special function to describe the terms of a partial cross section expansion in a compact and numerically well-described manner. In the non-relativistic thermal average

$$\langle\sigma v\rangle_{\rm NR} = \frac{2x^{3/2}}{\pi^{1/2}}\int_0^\infty \sigma v_{\rm lab}\epsilon^{1/2}e^{-x\epsilon}d\epsilon\ , \tag{23}$$

we rewrite the integral as

$$\int_0^\infty \frac{1}{s_0}{\rm Re}\left[\frac{i}{\epsilon_R + i\gamma_R - \epsilon}F(\epsilon)\epsilon^{1/2}e^{-x\epsilon}\right]d\epsilon\ . \tag{24}$$

Substituting the Taylor expansion $F(\epsilon) = \sum_{\ell=0}^\infty F^{(\ell)}\epsilon^\ell/\ell!$, we find

$$\langle\sigma v\rangle_{\rm NR} = \frac{2x^{3/2}\pi^{1/2}}{s_0}\sum_{\ell=0}^\infty \frac{F^{(\ell)}}{\ell!}{\rm Re}\left[\frac{i}{\pi}\int_0^\infty \frac{\epsilon^{\ell+1/2}e^{-x\epsilon}}{z_R-\epsilon}d\epsilon\right]\ , \tag{25}$$

where $z_R \equiv \epsilon_R + i\gamma_R$. The s- and p-wave terms of the above expansion can be written compactly as

$$\begin{aligned}\langle\sigma v\rangle_{\rm NR} \approx \frac{2x^{3/2}\pi^{1/2}}{s_0}\Big\{&F^{(0)}{\rm Re}\left[z_R^{1/2}w(x^{1/2}z_R^{1/2})\right]\\ &+F^{(1)}\left(\gamma_R\pi^{-1/2}x^{-1/2} + {\rm Re}\left[z_R^{3/2}w(x^{1/2}z_R^{1/2})\right]\right)\Big\}\ ,\end{aligned} \tag{26}$$

where

$$w(z) \equiv \frac{2iz}{\pi}\int_0^\infty \frac{e^{-t^2}}{z^2-t^2}dt = e^{-z^2}\left(1 + \frac{2i}{\sqrt{\pi}}\int_0^z e^{t^2}dt\right) \tag{27}$$

is the Faddeeva function. The first form in Eq. (27) is useful to derive Eq. (26), and the second form can be used to evaluate the function numerically and efficiently. In this work, numerical calculations were performed with the SciPy library [39] using the method of Ref. [40] to evaluate the Faddeeva function close to the real axis.

We now turn to the specific models we consider in this paper. For the case of scalar X annihilating to standard model final states through $XX \to A' \to \text{SM}$, the cross section takes the form

$$\sigma v_{\text{lab}} = \frac{16\pi\kappa^2\alpha\alpha_X}{3\left((s-m_{A'}^2)^2+m_{A'}^2\Gamma_{A'}^2\right)} \frac{\epsilon\left[m_e^2+2(1+\epsilon)m_X^2\right]\sqrt{1+\epsilon-m_e^2/m_X^2}}{(1+2\epsilon)\sqrt{1+\epsilon}\; B_e(2m_X\sqrt{1+\epsilon})} \,, \tag{28}$$

which implies

$$F(\epsilon) = \frac{16\pi\kappa^2\alpha\alpha_X}{3m_{A'}\Gamma_{A'}} \frac{\epsilon\left[m_e^2+2(1+\epsilon)m_X^2\right]\sqrt{1+\epsilon-m_e^2/m_X^2}}{(1+2\epsilon)\sqrt{1+\epsilon}\; B_e(2m_X\sqrt{1+\epsilon})} \,. \tag{29}$$

This cross section is p-wave suppressed, as indicated by the leading factor of ϵ. We therefore know that $F^{(0)}$ vanishes, and we can verify that

$$F^{(1)} = \frac{16\pi\kappa^2\alpha\alpha_X}{3m_{A'}\Gamma_{A'}} \frac{\left(m_e^2+2m_X^2\right)\sqrt{1-m_e^2/m_X^2}}{B_e(2m_X)} \,. \tag{30}$$

Given this, the thermally-averaged cross section is given by Eq. (26), and the thermal relic density and freezeout temperature can be determined by Eqs. (8) and (9).

For the pseudo-Dirac case, the cross section for annihilation through $\chi_1\chi_2 \to A' \to \text{SM}$ is

$$\begin{aligned}\sigma v_{\text{lab}} = {} & \frac{4\pi\kappa^2\alpha\alpha_X}{3s_0\left[(s-m_{A'}^2)^2+m_{A'}^2\Gamma_{A'}^2\right]} \\ & \times \frac{(3+2\epsilon)\left[(1+\epsilon)s_0+2m_e^2\right]\left[s_0(1+\epsilon)-4m_e^2\right]^{1/2}\left[s_0(1+\epsilon)-\Delta^2\right]^{1/2}}{(1+\epsilon)(1+2\epsilon)\; B_e(\sqrt{s_0(1+\epsilon)})} \,,\end{aligned} \tag{31}$$

which implies

$$F(\epsilon) = \frac{4\pi\kappa^2\alpha\alpha_X}{3s_0m_{A'}\Gamma_{A'}} \frac{(3+2\epsilon)\left[(1+\epsilon)s_0+2m_e^2\right]\left[s_0(1+\epsilon)-4m_e^2\right]^{1/2}\left[s_0(1+\epsilon)-\Delta^2\right]^{1/2}}{(1+\epsilon)(1+2\epsilon)\; B_e(\sqrt{s_0(1+\epsilon)})} \,. \tag{32}$$

This is an s-wave cross section, and it is easy to read off the constant term in the Taylor expansion of F:

$$F^{(0)} = \frac{4\pi\kappa^2\alpha\alpha_X}{s_0m_{A'}\Gamma_{A'}B_e(\sqrt{s_0})}(s_0+2m_e^2)(s_0-4m_e^2)^{1/2}(s_0-\Delta^2)^{1/2} \,. \tag{33}$$

This determines the leading contribution to the thermally-averaged cross section through Eq. (26).

There is an additional complication in the pseudo-Dirac case: when the dark sector consists of multiple nearly-degenerate species, we must include coannihilation factors in the thermally-averaged cross section [38] and the freezeout condition. The effective thermally-averaged cross section is

$$\langle\sigma v\rangle_{\text{eff}} = \frac{2(1+\Delta/m_X)^{3/2}e^{-x\Delta/m_X}}{\left[1+(1+\Delta/m_X)^{3/2}e^{-x\Delta/m_X}\right]^2}\langle\sigma v\rangle_{\text{NR}} \,. \tag{34}$$

The freezeout condition is modified to

$$\frac{63\times5^{1/2}x_f^{-1/2}e^{-x_f}g}{32\pi^3}\frac{g_{\text{eff}}^{1/2}}{h_{\text{eff}}}m_Xm_{\text{Pl}}\left[1+\left(1+\frac{\Delta}{m_X}\right)^{3/2}e^{-x_f\Delta/m_X}\right]\langle\sigma v\rangle_{\text{eff}} = 1 \,, \tag{35}$$

and the relic abundance is given by

$$\Omega_Xh^2 = 8.77\times10^{-11}\ \text{GeV}^{-2}\left[\overline{g_{\text{eff}}^{1/2}}\int_{x_f}^{x_0}\frac{\langle\sigma v\rangle_{\text{eff}}}{x^2}dx\right]^{-1} \,. \tag{36}$$

V. RESULTS

We present here the results of our analysis using the formalism of Sec. IV. Thermal relic contours for the benchmark, near-maximal perturbative value of the dark fine structure constant $\alpha_X = 0.5$ are shown in Fig. 1 for various values of ϵ_R. The contours for the non-degenerate case $m_{A'} = 3m_X$ agree within $\sim 10\%$ with those presented previously for scalar [33] and pseudo-Dirac [11] dark matter, which are shown as dotted curves. The minor discrepancy is due to a $\sim 10\%$ difference between the thermally-averaged cross section in the non-relativistic approximation used here and the relativistic thermally-averaged cross section used in Refs. [11, 33] at freeze-out temperatures near $x_f = 15$. For the degenerate case $\epsilon_R = 0.1$, as expected given the analytic estimate of Sec. III, the thermal targets for scalar (pseudo-Dirac) dark matter move to values of κ^2 that are four (two) orders of magnitude lower, relative to the $m_{A'} = 3m_X$ non-degenerate case.

The gray shaded regions in Fig. 1 are excluded by various combinations of current constraints from BaBar [7, 8], CRESST II [9], E137 [10, 11], LSND [11–14], and NA64 [15]. The CRESST II bounds are not applicable to pseudo-Dirac dark matter with $\Delta = 0.1\, m_X$, while exclusions from non-observation of excited state decays $\chi_2 \to \chi_1 e^+ e^-$ at E137 and LSND [11] apply only to pseudo-Dirac dark matter with $\Delta > 2m_e$. Observations of the CMB [1] exclude thermal relic Majorana dark matter below the 10 GeV mass range [41], but we include in Fig. 1 the resonant thermal targets for $\Delta = 0$ to illustrate the effect of a nonzero mass splitting. Note the thermal targets' stronger dependence on ϵ_R for smaller values of Δ. Also included in Fig. 1 are the projected sensitivities of planned accelerator-based dark photon and dark matter searches at BDX [11, 16, 17], Belle II [18], COHERENT [19, 20], DarkLight [21], LDMX [22], MiniBoone [11, 13, 14, 23], MMAPS [24], NA64 [25], PADME [26, 27], SHiP [28, 29], SBNe/SBNπ [30, 31], and VEPP-3 [32]. The excluded regions and future sensitivities assume $m_{A'} = 3m_X$. For comparison with the degenerate case contours with $m_{A'} \approx 2m_X$, these contours may be shifted up or down by $\mathcal{O}(1)$ factors. For a comprehensive overview of existing constraints and future experimental sensitivities, see Ref. [42].

Direct detection experiments can also probe these invisible dark photon scenarios. Although not searches for dark photons per se, they probe the $A'XX$ vertex that induces invisible A' decay through its role in inducing $X\,\mathrm{SM} \to X\,\mathrm{SM}$ scattering through a t-channel A'. To facilitate comparison with direct detection experiments, it is convenient [43, 44] to express the thermal relic parameter values in terms of

$$\bar{\sigma}_e = \frac{16\pi\mu_{X,e}^2 \alpha\kappa^2\alpha_X}{(m_{A'}^2 + \alpha^2 m_e^2)^2}\ , \tag{37}$$

where $\mu_{X,T}$ denotes the reduced mass of the dark matter-target system with $T = e$, nucleon, or nucleus. For the case of Majorana dark matter, the definition of $\bar{\sigma}_e$ includes an additional factor of $2(\mu_{X,T}^2/m_X^2)v_X^2$, where $v_X = 10^{-3}$ is the characteristic DM halo velocity.

In Fig. 2 we show the same thermal targets as in Fig. 1, but expressed in the $(m_X, \bar{\sigma}_e)$ parameter space and compared to current and proposed direct detection experiments. Fig. 2 includes current exclusions from XENON [45, 46], as well as projected regions of sensitivity [44, 45, 47–50] for CYGNUS HD-10, DAMIC-1K [51, 52], NEWS, PTOLEMY-G3, SENSEI [53], SuperCDMS [54, 55], UA$'$(1), and future experiments based on GaAs scintillators [47] superconducting aluminum, superfluid helium [56–60], color center production [61, 62], magnetic bubble chambers [63], scintillating bubble chambers [64], and bremsstrahlung in inelastic DM-nucleus scattering [65, 66]. Exclusions and regions of sensitivity for nuclear recoil experiments are converted into limits and projected sensitivities for $\bar{\sigma}_e$ using

$$\bar{\sigma}_e = 4\frac{\mu_{X,e}^2}{\mu_{X,N}^2}\sigma_N\ , \tag{38}$$

which makes it possible to compare the thermal targets and sensitivities of both electron and nuclear recoil experiments in the same parameter space. As in Fig. 1, the excluded regions and future sensitivities assume $m_{A'} = 3m_X$ and are reviewed in Ref. [42].

Comparing the thermal targets with the existing constraints and projected sensitivities, we see that for the scalar case and $\epsilon_R \sim 10\%$, the thermal target cannot be probed in any proposed accelerator or beam dump experiment. For the fermionic dark matter cases and $\epsilon_R \sim 10\%$, the thermal target is also beyond the reach of all proposed accelerator-based experiments, with the exception of LDMX, for which it is at the border of sensitivity, and becomes very challenging for smaller mass splittings Δ. For direct detection experiments, the thermal target for moderate degeneracy $\epsilon_R \sim 10\%$ is still within the projected reach of some far future experiments in the scalar case, but is beyond all proposed experiments in the Majorana case.

We also show results for smaller values of ϵ_R in Fig. 1. For greater degeneracies, the thermal target region moves to even lower values of κ^2. For $\epsilon_R \sim 10^{-6}$, for example, the thermal targets are essentially beyond all proposed accelerator and direct detection experiments for both the scalar and fermionic dark matter cases.

At first sight, the extreme suppression of the preferred values of κ^2 might be surprising, since the thermally-averaged cross section, for example, in Eq. (19), becomes independent of ϵ_R for $x_f \epsilon_R \ll 1$. However, for very small ϵ_R, the dark matter continues to annihilate long after freezeout as the universe cools. This is accounted for by the integral in Eq. (8), and that integral is sensitive to ϵ_R, even it is very small.

To understand this behavior, it is convenient to use the narrow width approximation. In the case that $\Gamma_{A'} \ll m_{A'}$ we can write the generic resonant cross section as

$$\sigma v_{\rm lab} \approx \frac{\pi}{s_0} F(\epsilon) \delta(\epsilon - \epsilon_R) \ , \tag{39}$$

which yields for the thermal average

$$\langle \sigma v \rangle_{\rm NR} \approx \frac{2\pi^{1/2} x^{3/2}}{s_0} \epsilon_R^{1/2} F(\epsilon_R) e^{-x\epsilon_R} \ . \tag{40}$$

We notice that in both the scalar and pseudo-Dirac cases, as long as $\Gamma_{\rm SM} \ll \Gamma_\phi, \Gamma_\chi$ and $\epsilon_R \ll 1$, the quantity $F(\epsilon_R)$ scales like $\epsilon_R^{-1/2}$. Therefore the thermally-averaged cross section's dependence on ϵ_R is contained entirely in the factor $\exp(-x\epsilon_R)$. This observation implies a simple relation between values of ϵ_R and κ that yield the correct relic abundance:

$$\Omega_X h^2 \propto \left[\int_{x_f}^{x_0} \frac{\kappa^2}{x^{1/2}} e^{-x\epsilon_R} \, dx \right]^{-1} \propto \frac{\sqrt{\epsilon_R}}{\kappa^2} \ . \tag{41}$$

We see that as $\epsilon_R \to 0$, a decrease of ϵ_R by an order of magnitude requires κ^2 to decrease by a factor of $\sqrt{10}$ to maintain the correct relic abundance.

What are the smallest possible values of ϵ_R? In the scalar dark matter case, as we lower ϵ_R, eventually the phase-space suppression of hidden sector decays will outweigh the kinetic mixing suppression of standard model decays, so that our assumption of invisible decays fails. Neglecting the electron mass, the requirement that the invisible width dominates implies

$$\Gamma_\phi \approx \frac{\alpha_X m_{A'}}{12} \epsilon_R^{3/2} \gtrsim \frac{\alpha m_{A'}}{3B_e} \kappa^2 \approx \Gamma_{\rm SM} \ . \tag{42}$$

It is clear, based on the power law dependence on ϵ_R, that this condition cannot hold simultaneously with the thermal relic constraint over all of parameter space. For a given α_X, there will be a minimum value of ϵ_R below which visible decays dominate the dark photon width. We find this minimum value to be $\epsilon_R^{\rm min} \approx 10^{-6}$ for $\alpha_X = 0.5$.

In contrast, in the pseudo-Dirac case, the invisible width condition is

$$\Gamma_\chi \approx \frac{\alpha_X m_{A'}}{3} \epsilon_R^{1/2} \gtrsim \frac{\alpha m_{A'}}{3B_e} \kappa^2 \approx \Gamma_{\rm SM} \ , \tag{43}$$

which follows the same scaling as the thermal relic condition. In the pseudo-Dirac case, then, it is possible to lower the thermal target region to arbitrarily low values of κ^2 by choosing the dark matter to be arbitrarily close to resonance. Put another way, enforcing the thermal relic constraint on a pseudo-Dirac dark sector "accidentally" fixes the ratio between the visible and invisible widths of the dark photon, so that the dual assumptions of mostly invisible dark photon decays and of thermal relic pseudo-Dirac dark matter may hold concurrently for all values of ϵ_R.

This is a remarkable result. It may be possible, in principle, to construct an experiment that can truly probe all of the thermal relic parameter space for perturbative theories of complex scalar dark matter coupled to a dark photon, but theories of fermionic dark matter may evade any such search by a fine-tuned choice of the dark sector masses.

The interesting behavior for highly degenerate cases may have interesting consequences in other contexts. For example, in the case of Kaluza-Klein dark matter [67, 68], level-1 fermionic dark matter with mass $m_{\rm KK}$ may annihilate through level-2 resonances with masses near $2m_{\rm KK}$, providing a rationale for high degeneracies. These resonances will impact thermal relic density calculations [69], but for extreme degeneracies, our results imply that there may also be interesting astrophysical signals from dark matter annihilation long after freeze out. Other interesting implications of resonances for such TeV-scale dark matter have been explored in Refs. [70–72].

VI. CONCLUSIONS

The absence of the discovery of WIMPs and other classic dark matter candidates has motivated many new dark matter candidates in recent years. Among those that are often seen as especially motivated are those that are in

thermal equilibrium with the standard model at early times, but then freeze out with the correct thermal relic density. The regions of model parameter space that give the desired relic density are "thermal targets" that provide important goals for new experimental searches.

In this study, we considered dark photon scenarios in which the dark photon decays invisibly to dark matter through $A' \to XX$. Such scenarios can be probed by experiments searching for missing mass, energy, or momentum. For generic A' and X masses, proposed experiments, notably LDMX, are projected to be sensitive to the thermal target parameter space. Direct detection experiments may also be sensitive to these scenarios by searches for $X\,\mathrm{SM} \to X\,\mathrm{SM}$ induced by t-channel A' exchange.

Of course, in such scenarios, since $m_{A'} > 2m_X$, the annihilation process $XX \to A' \to \mathrm{SM}$ can be enhanced by the A' resonance when the initial state dark matter particles have sufficient kinetic energies. In this work, we have found that for $m_{A'} - 2m_X \sim 0.1\, m_X$, the resonance implies a kinematic enhancement of the annihilation rate for scalar (pseudo-Dirac) dark matter of four (two) orders of magnitude, or, alternatively, the thermal target parameter space moves to values of the kinetic mixing κ^2 that are four (two) orders of magnitude smaller. We derived these results using a simple analytic estimate in Sec. III and through a more accurate numerical analysis in Sec. IV.

The resulting thermal targets are shown in Figs. 1 and 2. Even for the case of a 10% degeneracy $m_{A'} - 2m_X \sim 0.1\, m_X$, we find that the thermal targets are very difficult to probe. For the scalar case, the thermal target is below the projected reach of LDMX and all other proposed accelerator experiments. For the pseudo-Dirac case, the thermal target is also beyond the reach of all proposed accelerator-based experiments, with the exception of LDMX, for which it is at the border of sensitivity, and becomes very challenging for smaller mass splittings. Direct detection experiments do slightly better, as the thermal target for $\epsilon_R \sim 10\%$ is still within the projected reach of some far future experiments in the scalar case, but the thermal targets are still beyond all proposed experiments in the Majorana case.

For even greater degeneracies, with $m_{A'} - 2m_X \ll 0.1\, m_X$, the thermal targets move to even lower values of κ^2. For $\epsilon_R \sim 10^{-6}$, the thermal targets are essentially beyond all proposed accelerator and direct detection experiments for both the scalar and fermionic dark matter cases.

Interestingly, for the case of scalar dark matter, for extreme degeneracies, the condition that the A' decays dominantly invisibly becomes inconsistent with the thermal relic condition. This establishes a floor at $m_{A'} - 2m_X \sim 10^{-6}\, m_X$ that is roughly four orders of magnitude in κ^2 below the projected reach of LDMX, but which is the ultimate goal for an experiment that can probe the entire thermal target region. The floor of the scalar dark matter parameter space may be accessible to future superfluid helium experiments. Unfortunately, for pseudo-Dirac dark matter, there is no such floor for the thermal target. Of course, barring some more fundamental rationale, the fine-tuning required for such degeneracies is extreme, and ultimately other constraints will apply.

Acknowledgments

We are grateful to Anthony DiFranzo, Bertrand Echenard, Eder Izaguirre, Yoni Kahn, Gopolang Mohlabeng, Brian Shuve, and, especially, Rouven Essig and Gordan Krnjaic for helpful discussions. This work is supported in part by NSF Grant No. PHY-1620638. J.L.F. is supported in part by Simons Investigator Award #376204, and J.S. is supported in part by Department of Education GAANN Grant No. P200A150121 at UC Irvine.

[1] **Planck** Collaboration, P. A. R. Ade *et al.*, "Planck 2015 results. XIII. Cosmological parameters," *Astron. Astrophys.* **594** (2016) A13, arXiv:1502.01589 [astro-ph.CO].

[2] J. L. Feng and J. Kumar, "The WIMPless Miracle: Dark-Matter Particles without Weak-Scale Masses or Weak Interactions," *Phys. Rev. Lett.* **101** (2008) 231301, arXiv:0803.4196 [hep-ph].

[3] L. B. Okun, "Limits of electrodynamics: paraphotons?," *Sov. Phys. JETP* **56** (1982) 502. [Zh. Eksp. Teor. Fiz. 83, 892 (1982)].

[4] B. Holdom, "Two U(1)'s and Epsilon Charge Shifts," *Phys. Lett.* **B166** (1986) 196–198.

[5] C. Boehm and P. Fayet, "Scalar dark matter candidates," *Nucl. Phys.* **B683** (2004) 219–263, arXiv:hep-ph/0305261 [hep-ph].

[6] M. Pospelov, "Secluded U(1) below the weak scale," *Phys. Rev.* **D80** (2009) 095002, arXiv:0811.1030 [hep-ph].

[7] **BaBar** Collaboration, J. P. Lees *et al.*, "Search for a Dark Photon in e^+e^- Collisions at BaBar," *Phys. Rev. Lett.* **113** (2014) 201801, arXiv:1406.2980 [hep-ex].

[8] **BaBar** Collaboration, J. P. Lees *et al.*, "Search for invisible decays of a dark photon produced in e+e- collisions at BaBar," arXiv:1702.03327 [hep-ex].

[9] **CRESST** Collaboration, G. Angloher *et al.*, "Results on light dark matter particles with a low-threshold CRESST-II detector," *Eur. Phys. J.* **C76** (2016) 25, arXiv:1509.01515 [astro-ph.CO].

[10] B. Batell, R. Essig, and Z. Surujon, "Strong Constraints on Sub-GeV Dark Sectors from SLAC Beam Dump E137," *Phys. Rev. Lett.* **113** (2014) 171802, arXiv:1406.2698 [hep-ph].

[11] E. Izaguirre, Y. Kahn, G. Krnjaic, and M. Moschella, "Testing Light Dark Matter Coannihilation With Fixed-Target Experiments," arXiv:1703.06881 [hep-ph].

[12] **LSND** Collaboration, C. Athanassopoulos *et al.*, "The Liquid scintillator neutrino detector and LAMPF neutrino source," *Nucl. Instrum. Meth.* **A388** (1997) 149–172, arXiv:nucl-ex/9605002 [nucl-ex].

[13] P. deNiverville, M. Pospelov, and A. Ritz, "Observing a light dark matter beam with neutrino experiments," *Phys. Rev.* **D84** (2011) 075020, arXiv:1107.4580 [hep-ph].

[14] P. deNiverville, C.-Y. Chen, M. Pospelov, and A. Ritz, "Light dark matter in neutrino beams: production modelling and scattering signatures at MiniBooNE, T2K and SHiP," *Phys. Rev.* **D95** no. 3, (2017) 035006, arXiv:1609.01770 [hep-ph].

[15] **NA64** Collaboration, D. Banerjee *et al.*, "Search for invisible decays of sub-GeV dark photons in missing-energy events at the CERN SPS," *Phys. Rev. Lett.* **118** (2017) 011802, arXiv:1610.02988 [hep-ex].

[16] **BDX** Collaboration, M. Battaglieri *et al.*, "Dark Matter Search in a Beam-Dump eXperiment (BDX) at Jefferson Lab," arXiv:1607.01390 [hep-ex].

[17] **BDX** Collaboration, M. Bond, "Light Dark Matter search in a beam-dump experiment: BDX at Jefferson Lab," *EPJ Web Conf.* **142** (2017) 01005.

[18] C. Hearty, "Dark Sector Searches at B-factories and outlook for Belle II," 2017. https://indico.fnal.gov/getFile.py/access?contribId=123&sessionId=9&resId=0&materialId=slides&confId=13702.

[19] "COHERENT experiment." http://sites.duke.edu/coherent.

[20] P. deNiverville, M. Pospelov, and A. Ritz, "Light new physics in coherent neutrino-nucleus scattering experiments," *Phys. Rev.* **D92** (2015) 095005, arXiv:1505.07805 [hep-ph].

[21] J. Balewski *et al.*, "The DarkLight Experiment: A Precision Search for New Physics at Low Energies," 2014. arXiv:1412.4717 [physics.ins-det].

[22] "LDMX experiment." https://confluence.slac.stanford.edu/display/MME/Light+Dark+Matter+Experiment.

[23] **MiniBooNE** Collaboration, A. A. Aguilar-Arevalo *et al.*, "Dark Matter Search in a Proton Beam Dump with MiniBooNE," *Phys. Rev. Lett.* **118** (2017) 221803, arXiv:1702.02688 [hep-ex].

[24] J. Alexander, "Dark Photon Search in e+e- Annihilation," 2016. https://indico.cern.ch/event/507783/contributions/2150181/attachments/1266367/1874844/SLAC-MMAPS-alexander.pdf.

[25] S. N. Gninenko, "NA64++," 2017. https://indico.cern.ch/event/608491/contributions/2457799/attachments/1420197/2176021/NA64_0317.pdf.

[26] M. Raggi and V. Kozhuharov, "Proposal to Search for a Dark Photon in Positron on Target Collisions at DAΦNE Linac," *Adv. High Energy Phys.* **2014** (2014) 959802, arXiv:1403.3041 [physics.ins-det].

[27] M. Raggi, V. Kozhuharov, and P. Valente, "The PADME experiment at LNF," *EPJ Web Conf.* **96** (2015) 01025, arXiv:1501.01867 [hep-ex].

[28] S. Alekhin *et al.*, "A facility to Search for Hidden Particles at the CERN SPS: the SHiP physics case," *Rept. Prog. Phys.* **79** (2016) 124201, arXiv:1504.04855 [hep-ph].

[29] **SHiP** Collaboration, M. Anelli *et al.*, "A facility to Search for Hidden Particles (SHiP) at the CERN SPS," arXiv:1504.04956 [physics.ins-det].

[30] **LAr1-ND, ICARUS-WA104, MicroBooNE** Collaboration, M. Antonello *et al.*, "A Proposal for a Three Detector Short-Baseline Neutrino Oscillation Program in the Fermilab Booster Neutrino Beam," arXiv:1503.01520 [physics.ins-det].

[31] R. Van de Water, "Future Sub-GeV Dark Matter Searches with Proton Fixed Targets at FNAL." https://indico.fnal.gov/getFile.py/access?contribId=157&sessionId=6&resId=10&materialId=minutes&confId=13702.

[32] B. Wojtsekhowski, D. Nikolenko, and I. Rachek, "Searching for a new force at VEPP-3," arXiv:1207.5089 [hep-ex].

[33] E. Izaguirre, G. Krnjaic, P. Schuster, and N. Toro, "Analyzing the Discovery Potential for Light Dark Matter," *Phys. Rev. Lett.* **115** (2015) 251301, arXiv:1505.00011 [hep-ph].

[34] M. Buschmann, J. Kopp, J. Liu, and P. A. N. Machado, "Lepton Jets from Radiating Dark Matter," *JHEP* **07** (2015) 045, arXiv:1505.07459 [hep-ph].

[35] D. Tucker-Smith and N. Weiner, "Inelastic dark matter," *Phys. Rev.* **D64** (2001) 043502, arXiv:hep-ph/0101138 [hep-ph].

[36] E. Izaguirre, G. Krnjaic, and B. Shuve, "Discovering Inelastic Thermal-Relic Dark Matter at Colliders," *Phys. Rev.* **D93** (2016) 063523, arXiv:1508.03050 [hep-ph].

[37] P. Gondolo and G. Gelmini, "Cosmic abundances of stable particles: Improved analysis," *Nucl. Phys.* **B360** (1991) 145–179.

[38] K. Griest and D. Seckel, "Three exceptions in the calculation of relic abundances," *Phys. Rev.* **D43** (1991) 3191–3203.

[39] E. Jones, T. Oliphant, P. Peterson, *et al.*, "SciPy: Open source scientific tools for Python," 2001–. http://www.scipy.org. [Online; accessed 6/10/2017].

[40] M. R. Zaghloul and A. N. Ali, "Algorithm 916: Computing the Faddeyeva and Voigt Functions," *ACM Trans. Math. Softw.* **38** (Jan., 2012) 15:1–15:22.

[41] T. R. Slatyer, "Indirect dark matter signatures in the cosmic dark ages. I. Generalizing the bound on s-wave dark matter annihilation from Planck results," *Phys. Rev.* **D93** no. 2, (2016) 023527, arXiv:1506.03811 [hep-ph].

[42] M. Battaglieri *et al.*, "US Cosmic Visions: New Ideas in Dark Matter 2017: Community Report," arXiv:1707.04591 [hep-ph].

[43] R. Essig, J. Mardon, and T. Volansky, "Direct Detection of Sub-GeV Dark Matter," *Phys. Rev.* **D85** (2012) 076007, arXiv:1108.5383 [hep-ph].

[44] R. Essig, M. Fernandez-Serra, J. Mardon, A. Soto, T. Volansky, and T.-T. Yu, "Direct Detection of sub-GeV Dark Matter with Semiconductor Targets," *JHEP* **05** (2016) 046, arXiv:1509.01598 [hep-ph].

[45] R. Essig, A. Manalaysay, J. Mardon, P. Sorensen, and T. Volansky, "First Direct Detection Limits on sub-GeV Dark Matter from XENON10," *Phys. Rev. Lett.* **109** (2012) 021301, arXiv:1206.2644 [astro-ph.CO].

[46] R. Essig, T. Volansky, and T.-T. Yu, "New Constraints and Prospects for sub-GeV Dark Matter Scattering off Electrons in Xenon," arXiv:1703.00910 [hep-ph].

[47] S. Derenzo, R. Essig, A. Massari, A. Soto, and T.-T. Yu, "Direct Detection of sub-GeV Dark Matter with Scintillating Targets," *Phys. Rev.* **D96** (2017) 016026, arXiv:1607.01009 [hep-ph].

[48] Y. Hochberg, Y. Kahn, M. Lisanti, C. G. Tully, and K. M. Zurek, "Directional detection of dark matter with two-dimensional targets," *Phys. Lett.* **B772** (2017) 239–246, arXiv:1606.08849 [hep-ph].

[49] Y. Hochberg, M. Pyle, Y. Zhao, and K. M. Zurek, "Detecting Superlight Dark Matter with Fermi-Degenerate Materials," *JHEP* **08** (2016) 057, arXiv:1512.04533 [hep-ph].

[50] Y. Hochberg, Y. Zhao, and K. M. Zurek, "Superconducting Detectors for Superlight Dark Matter," *Phys. Rev. Lett.* **116** (2016) 011301, arXiv:1504.07237 [hep-ph].

[51] **DAMIC** Collaboration, A. Aguilar-Arevalo *et al.*, "Search for low-mass WIMPs in a 0.6 kg day exposure of the DAMIC experiment at SNOLAB," *Phys. Rev.* **D94** (2016) 082006, arXiv:1607.07410 [astro-ph.CO].

[52] **DAMIC** Collaboration, A. Aguilar-Arevalo *et al.*, "First Direct-Detection Constraints on eV-Scale Hidden-Photon Dark Matter with DAMIC at SNOLAB," *Phys. Rev. Lett.* **118** (2017) 141803, arXiv:1611.03066 [astro-ph.CO].

[53] J. Tiffenberg, M. Sofo-Haro, A. Drlica-Wagner, R. Essig, Y. Guardincerri, S. Holland, T. Volansky, and T.-T. Yu, "Single-electron and single-photon sensitivity with a silicon Skipper CCD," arXiv:1706.00028 [physics.ins-det].

[54] **SuperCDMS** Collaboration, R. Agnese *et al.*, "Search for Low-Mass Weakly Interacting Massive Particles with SuperCDMS," *Phys. Rev. Lett.* **112** (2014) 241302, arXiv:1402.7137 [hep-ex].

[55] **SuperCDMS** Collaboration, R. Agnese *et al.*, "New Results from the Search for Low-Mass Weakly Interacting Massive Particles with the CDMS Low Ionization Threshold Experiment," *Phys. Rev. Lett.* **116** (2016) 071301, arXiv:1509.02448 [astro-ph.CO].

[56] K. Schutz and K. M. Zurek, "Detectability of Light Dark Matter with Superfluid Helium," *Phys. Rev. Lett.* **117** (2016) 121302, arXiv:1604.08206 [hep-ph].

[57] S. Knapen, T. Lin, and K. M. Zurek, "Light Dark Matter in Superfluid Helium: Detection with Multi-excitation Production," *Phys. Rev.* **D95** (2017) 056019, arXiv:1611.06228 [hep-ph].

[58] W. Guo and D. N. McKinsey, "Concept for a dark matter detector using liquid helium-4," *Phys. Rev.* **D87** (2013) 115001, arXiv:1302.0534 [astro-ph.IM].

[59] F. W. Carter, S. A. Hertel, M. J. Rooks, D. N. McKinsey, and D. E. Prober, "Toward the In Situ Detection of Individual He2 Excimers Using a Ti TES in Superfluid Helium," *IEEE Transactions an Applied Superconductivity* **25** (2015) 2100707.

[60] H. J. Maris, G. M. Seidel, and D. Stein, "Dark Matter Detection Using Helium Evaporation and Field Ionization," arXiv:1706.00117 [astro-ph.IM].

[61] R. Essig, J. Mardon, O. Slone, and T. Volansky, "Detection of sub-GeV Dark Matter and Solar Neutrinos via Chemical-Bond Breaking," *Phys. Rev.* **D95** (2017) 056011, arXiv:1608.02940 [hep-ph].

[62] R. Budnik, O. Chesnovsky, O. Slone, and T. Volansky, "Direct Detection of Light Dark Matter and Solar Neutrinos via Color Center Production in Crystals," arXiv:1705.03016 [hep-ph].

[63] P. C. Bunting, G. Gratta, T. Melia, and S. Rajendran, "Magnetic Bubble Chambers and Sub-GeV Dark Matter Direct Detection," *Phys. Rev.* **D95** (2017) 095001, arXiv:1701.06566 [hep-ph].

[64] D. Baxter *et al.*, "First Demonstration of a Scintillating Xenon Bubble Chamber for Detecting Dark Matter and Coherent Elastic Neutrino-Nucleus Scattering," *Phys. Rev. Lett.* **118** (2017) 231301, arXiv:1702.08861 [physics.ins-det].

[65] C. Kouvaris and J. Pradler, "Probing sub-GeV Dark Matter with conventional detectors," *Phys. Rev. Lett.* **118** (2017) 031803, arXiv:1607.01789 [hep-ph].

[66] C. McCabe, "New constraints and discovery potential of sub-GeV dark matter with xenon detectors," *Phys. Rev.* **D96** (2017) 043010, arXiv:1702.04730 [hep-ph].

[67] G. Servant and T. M. P. Tait, "Is the lightest Kaluza-Klein particle a viable dark matter candidate?," *Nucl. Phys.* **B650** (2003) 391–419, arXiv:hep-ph/0206071 [hep-ph].

[68] H.-C. Cheng, J. L. Feng, and K. T. Matchev, "Kaluza-Klein dark matter," *Phys. Rev. Lett.* **89** (2002) 211301, arXiv:hep-ph/0207125 [hep-ph].

[69] M. Kakizaki, S. Matsumoto, Y. Sato, and M. Senami, "Significant effects of second KK particles on LKP dark matter physics," *Phys. Rev.* **D71** (2005) 123522, arXiv:hep-ph/0502059 [hep-ph].

[70] D. Feldman, Z. Liu, and P. Nath, "PAMELA Positron Excess as a Signal from the Hidden Sector," *Phys. Rev.* **D79** (2009) 063509, arXiv:0810.5762 [hep-ph].

[71] M. Ibe, H. Murayama, and T. T. Yanagida, "Breit-Wigner Enhancement of Dark Matter Annihilation," *Phys. Rev.* **D79** (2009) 095009, arXiv:0812.0072 [hep-ph].

[72] W.-L. Guo and Y.-L. Wu, "Enhancement of Dark Matter Annihilation via Breit-Wigner Resonance," *Phys. Rev.* **D79** (2009) 055012, arXiv:0901.1450 [hep-ph].

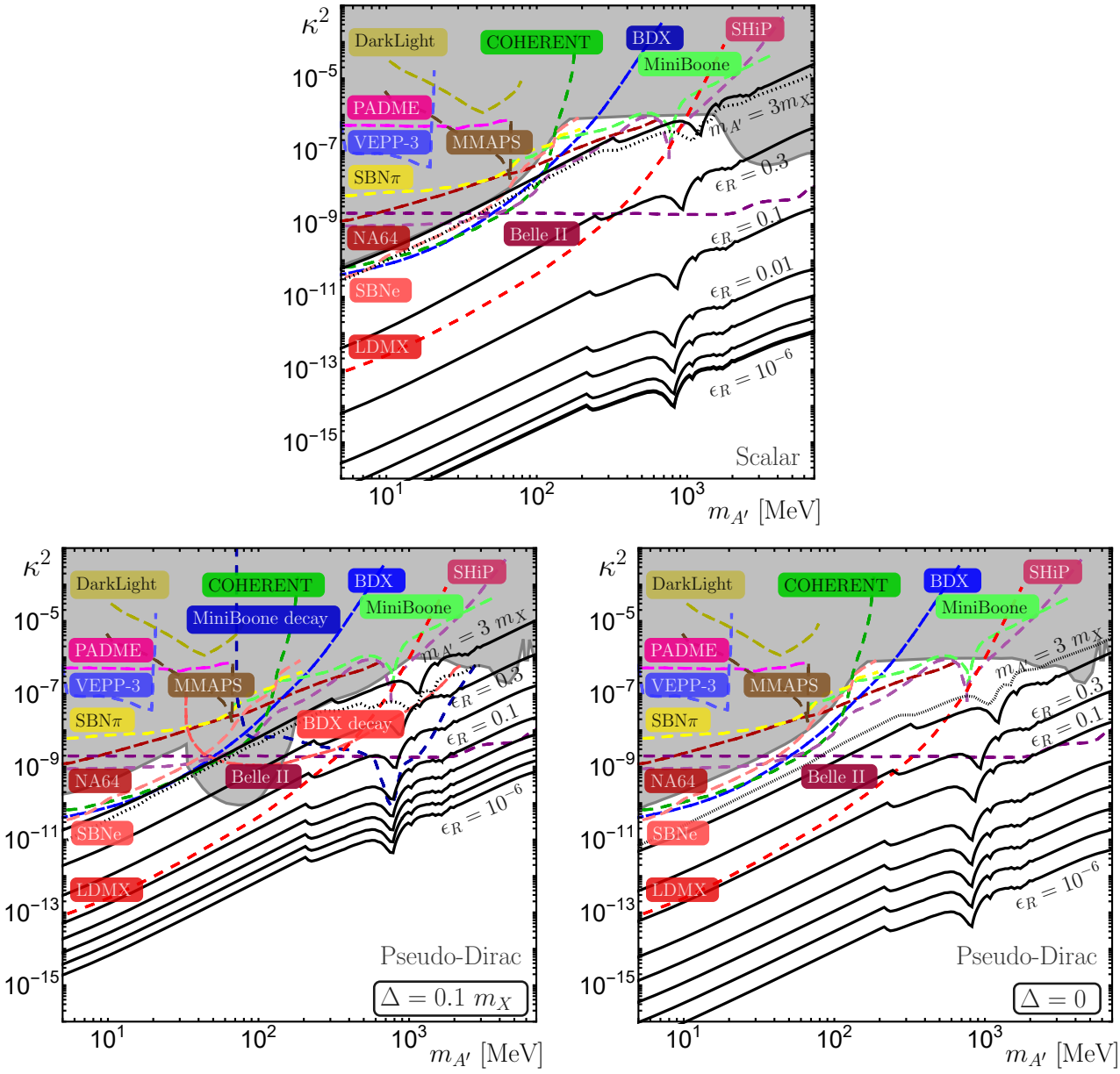

FIG. 1: **Thermal targets and accelerator search experiments.** Solid Black Contours: Thermal target contours in dark photon parameter space $(m_{A'}, \kappa^2)$ for $\alpha_X = 0.5$ in the non-degenerate cases with $m_{A'} = 3m_X$ and $\epsilon_R \equiv (m_{A'}^2 - 4m_X^2)/(4m_X^2) = 0.3$, and in the degenerate cases with $\epsilon_R = 10^{-n}$, where $n = 1, 2, \ldots 6$. In the scalar case (top) the thermal relic contours reach a floor near $\epsilon_R = 10^{-6}$, where the thermal relic abundance requirement becomes inconsistent with the requirement that the dark photon decay is dominantly invisible. The $\epsilon_R = 10^{-5}$ contour is displayed in this plot, but is close enough to the $\epsilon_R = 10^{-6}$ contour that they appear to overlap. In the pseudo-Dirac case (bottom) the thermal relic contours extend to arbitrarily low values of κ^2 with appropriate choice of ϵ_R, but we display only a small number of contours to avoid clutter. In the bottom left panel, the mass splitting is $\Delta = 0.1\, m_X$, and these models evade direct detection bounds. In the bottom right panel, $\Delta = 0$, which illustrates the effect of decreasing Δ on the thermal target regions. Dotted Black Contours: Thermal target contours for $m_{A'} = 3m_X$ from relativistic treatments of freeze-out for the scalar [33] and pseudo-Dirac [11] cases. Gray Shaded: Regions excluded by current bounds (see text). Dashed Contours: Projected reaches of proposed dark photon and dark matter accelerator searches (see text).

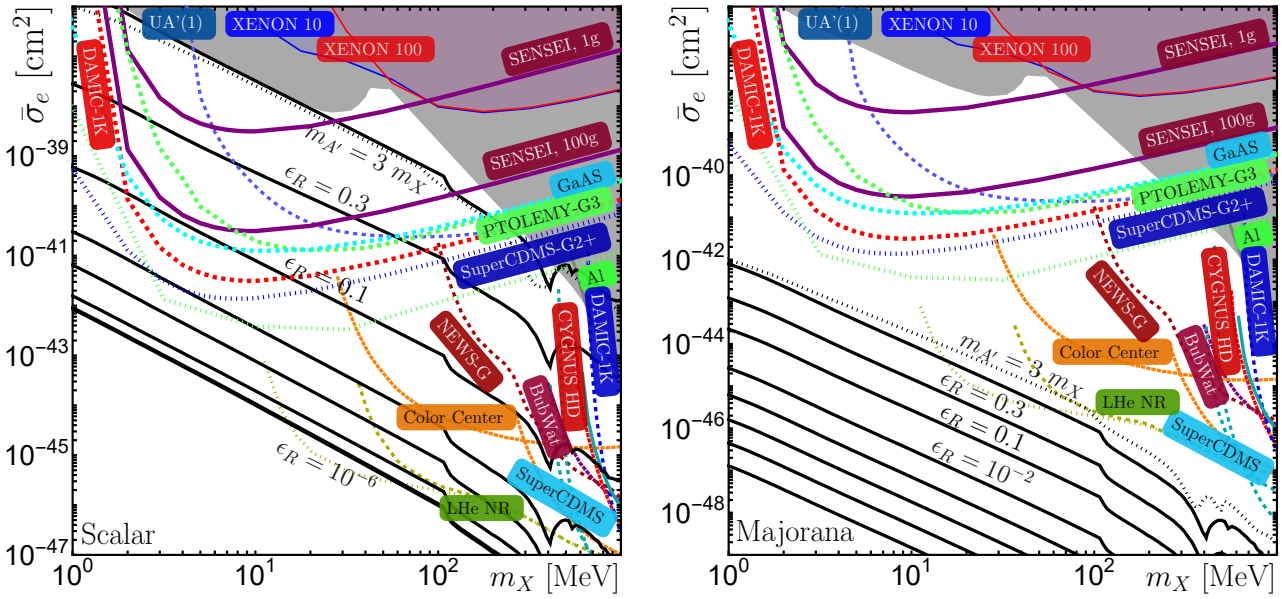

FIG. 2: **Thermal targets and direct detection search experiments.** Solid Black Contours: Thermal target contours as in Fig. 1, but in the direct detection parameter space $(m_X, \bar{\sigma}_e)$, where $\bar{\sigma}_e = (16\pi\mu_{X,e}^2\alpha\kappa^2\alpha_X)/(m_{A'}^2 + \alpha^2 m_e^2)^2$ (see text). In the scalar case (left) a resonantly annihilating thermal relic may still be within reach of future nuclear recoil experiments. In the right panel we show only the lines for Majorana DM-nuclear scattering, with $m_T = 0.936$ GeV; the thermal targets for DM-electron scattering scale approximately with the target mass squared, placing them far out of reach of current and proposed experiments. Dotted Black Contours: Relativistic thermal relic contours, as in Fig. 1. Gray Shaded: Regions excluded by current bounds (see text). Colored Contours: Projected reaches of proposed direct detection experiments (see text).